

Metal coating effect on thermal diffusivity of single-walled carbon nanotube

Shuhei Inoue <sup>a, \*</sup> and Yukihiro Matsumura <sup>a</sup>

*<sup>a</sup> Energy and Environmental Division, Faculty of Engineering, Hiroshima  
University*

*1-4-1 Kagamiyama, Higashi-Hiroshima 739-8527, Japan*

Abstract

Recently a functionalized single-walled carbon nanotube (SWCNT) that is modified by metal atoms was experimentally developed. Single-walled carbon nanotube is known to exhibit exceptional thermal conductivity; however, there is no report about a functionalized SWCNT. In this study, thermal diffusivity of metal-coated SWCNT was derived using molecular dynamics. Consequently, thermal diffusivity exhibited ten times smaller than uncoated SWCNT. On the other hand, the heat conduction on the metal layer was observed as the shape of shoulder on the thermal time response and it was found that this contribution was not small for a short-length SWCNT.

\* Corresponding Author. Fax: +81-82-424-5923.

*E-mail address:* shu18@hiroshima-u.ac.jp (S. Inoue).

## 1. Introduction

A single-walled carbon nanotube (SWCNT) [1] has a unique quasi one-dimensional structure and strong  $sp^2$  bonds, which make it a potentially useful material in many applications. Because of the development of mass production methods [2] and separation techniques [3], the application of SWCNTs has become a reality in the recent years.

The thermal property of SWCNT is quite interesting. The heat conduction is expressed by phonon transportation and electron transportation. Normally, metallic substances have large thermal conductivity, because the electron contribution is large; however, it is expected that SWCNT has much larger thermal conductivity than metallic substances even when the SWCNT is semi conducting. Owing to the strong bonds among carbon atoms, the heat conduction is occurred by phonon transportation. Because the ratio of thermal conductivity and electrical conductivity ( $\lambda / \sigma T$ ) is far from the Wiedemann-Franz law, the main factor of the heat transportation is phonon even for a metallic SWCNT [4]. One of the most interesting phenomena occurred in heat conduction of SWCNT is that the thermal conductivity of

SWCNT depends on its length. For example, when the dominant factor of heat conduction is phonon in a certain material, if its representative length is shorter enough than the phonon mean free path, the phonon is never dispersed. Consequently, there is no thermal resistance ( $R$  [ $\text{m}^2\text{K} / \text{W}$ ]) based on the dispersion; thus, the thermal conductivity ( $\lambda = L / R$  [ $\text{W} / \text{mK}$ ]), which is expressed by the reciprocal number of the thermal resistance, must be proportional to its length.

The developments of functionalized CNTs [5-20] have been reported and at present there has been more interest in using together with metal or metal matrix [10-20]. Furthermore, even SWCNTs are functionalized inorganically by using certain metal species and not organically by replacing carbon atoms with atoms of other elements such as nitrogen. Zhang et al. [21] functionalized SWCNTs by coating individual SWCNT with certain metal species; further, Ishikawa et al. [22] functionalized SWCNTs by depositing metal atoms onto vertically aligned SWCNT films. These techniques of SWCNT functionalization assist in having an affinity for conventional materials and/or devices, and controlling its electric conductivity, which cannot be directly controlled during its synthesis; further, they extend the

scope of application of SWCNTs. However, at present, there is no guarantee that the preservation of the exceptional physical properties such as the thermal conductivity and physical strength. Molecular dynamics simulation can be a great tool for elucidating these problems and makes clear the phenomena. Because functionalization of an SWCNT can disturb pure  $sp^2$  bonds, the physical strength and thermal conductivity of metal-coated SWCNTs are expected to be comparatively lower than those of an uncoated one. As found in our previous study, the physical strength becomes lower by 30% [23]. The physical properties [24] or thermal properties of SWCNT and/or interfaces between SWCNT and substances [25] are also quite interesting issues. In this study, we focused on thermal diffusivity of SWCNT and its non-Fourier behavior, which is always accompanied by ultra short time length thermal response problem [26]. Consequently, we find that the thermal diffusivity of the metal-coated SWCNT decreases but the heat conduction in metal layer exhibits comparably large amount for the short-length metal-coated SWCNT that might be expected compensating for the decrease in thermal diffusivity a little. On the other hand, for the long-length SWCNT, the thermal conductivity is originally much larger than

conventional materials; thus, metal-coated SWCNT can be a superior material even if its thermal conductivity becomes smaller due to metal coating.

## 2. Method

Molecular dynamics simulations were performed for nickel-coated and uncoated SWCNTs (lengths of 50 – 3000 Å, (5, 5) chirality). The velocity Verlet method is employed to integrate the classical equation of motion with a time step of 0.5 fs. Referring to our previous study [27], nickel can cover the SWCNT most smoothly among titanium, gold, iron, and nickel that were tried in our MD simulation; thus, nickel is most adequate material to examine its coating effect on physical properties. The potential functions for treating transition metal atoms have already developed such as Morse type [28], Finnis-Sinclair [29], embedded atom model [30], and so forth. On the other hand, there are no reliable classical potential functions to express carbon-metal interaction except for ReaxFF [31] and many-body potential functions employed in this study. Unlike traditional force field methods, ReaxFF seems to express chemical reaction, particularly, hydrocarbon reactions, transition-metal-catalyzed nanotube formation because that

allows for continuous bond formation/breaking. However, in this study, as we would like to express CNT-coating and its thermodynamic property, we employed the other potential function, which described below and can express local structure well. The carbon-carbon interaction was expressed using the Brenner-Tersoff potential [32]; its simplified form [33] is as follows in Eqs. (1) – (8):

$$E = V_R - V_A \quad (1)$$

$$V_R = \frac{D_e}{S-1} \exp\{-\beta\sqrt{2S}(r - R_e)\} \quad (2)$$

$$V_A = B^* \frac{D_e S}{S-1} \exp\{1 + b(N^C - 1)\}^\delta \quad (3)$$

$$D_e = D_{e1} + D_{e2} \exp\{-C_D(N^M - 1)\} \quad (4)$$

$$R_e = R_{e1} - R_{e2} \exp\{-C_R(N^M - 1)\} \quad (5)$$

$$f(r) = \begin{cases} 1 & (r < R_1) \\ 0.5 \cdot \left(1 + \cos \frac{r - R_1}{R_2 - R_1} \pi\right) & (R_1 < r < R_2) \\ 0 & (R_2 < r) \end{cases} \quad (6)$$

$$N_i^C = 1 + \sum_{carbon} f(r_{ik}) \quad (7)$$

$$N_i^M = 1 + \sum_{metal} f(r_{ik}) \quad (8)$$

In the above equations,  $r$  denotes the distance between two atoms, and  $V_R$  and  $V_A$  denote the Morse-type potential for the repulsion and attraction terms, respectively.  $R_e$  denotes the equilibrium bond length, and  $D_e$  is the potential depth at  $r = R_e$ .  $S$  represents the ratio of the effective repulsion to attraction.  $N_i^C$  and  $N_i^M$  are the coordination numbers derived from the cut-off function  $f(r)$ . The nickel–nickel and carbon–nickel interactions were expressed using Brenner type–bond order potential function [34], which considers the coordination numbers of nickel and carbon but not the angular effects of those. The nickel–coated SWCNTs were prepared by continuous deposition of small nickel cluster (Ni13) onto the sidewall of SWCNT with a deposition energy of 10 meV [35], and fully annealed by taking enough relaxation time, because the size of Ni13 is quite

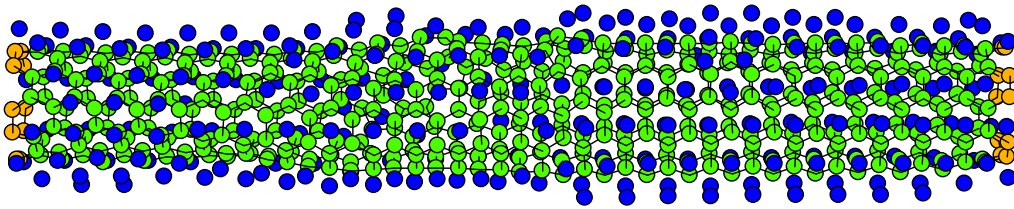


Fig. 1 Example of calculated object (C480 with Ni269). The SWCNT is completely covered with nickel atoms (blue).

comparable to the real clusters, which appear in vacuum deposition process. The periodic boundary condition was employed, but as both the ends of the SWCNT are fixed, the boundary condition is not essential for this simulation. Concerning to the mechanism for phenomena of depositing metal species onto SWCNT sidewall is discussed in above-mentioned paper; thus, we described a little about it. In this simulation, a metal-coated SWCNT is expressed by smoothly covered with half the number of nickel, as there are carbon atoms. This resulted in the formation of approximately two layers on each SWCNT, as shown in Fig. 1. Because the most stable position for the nickel atom is the center of hexagonal carbon network as shown Fig. 2, to cover by one layer almost one-third number of nickel is enough. Here, to express the experimental condition properly, we employed the SWCNT partially covered by two layers. Why we do not prepare the strictly one layer coated SWCNT is to express more practical surface and to exclude inessential enhancement of physical properties owing to the perfect crystallinity of metal associated SWCNT surface. Consequently, the number of layer did not affect the thermal diffusivity; otherwise, this effect was not shown in the thermal response at least.

An SWCNT is a quasi one-dimensional structure. Therefore, as shown Eq. (2), its thermal diffusivity ( $\alpha$ ) can be derived by fitting the temperature profile in SWCNT to the one-dimensional non-Fourier heat conduction equation with two relaxation timescales ( $\tau_1, \tau_2$ ). The thermal diffusivity is derived at an arbitrary time ( $t = t_l$ ) when heat does not propagate to both the ends to avoid from the heat reflection and unintentional boundary effect.

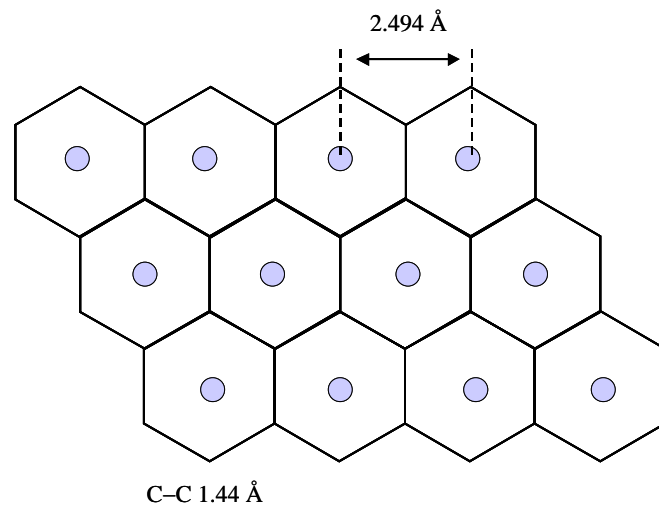


Fig. 2 Schematic of the position of nickel deposition onto SWCNT sidewall (expressed using unfolded graphite sheet). The distance of nickel ( $2.494\ \text{\AA}$ ) is quite comparable to the equilibrium bond length for Ni-Ni.

$$\tau_1 \frac{\partial^2 T}{\partial t^2} + \frac{\partial T}{\partial t} = \alpha \left( \nabla^2 T + \tau_2 \frac{\partial}{\partial t} \nabla^2 T \right) \quad (2)$$

Heat propagates by giving an instant temperature profile around at the center of SWCNT, as shown in Eq. (3). A simplified calculation system is shown in Fig. 3.

$$T(n) = T_0 \exp \left\{ -\varepsilon \cdot \left( \frac{n - 0.5n_0}{n_0} \right)^2 \right\} \quad (3)$$

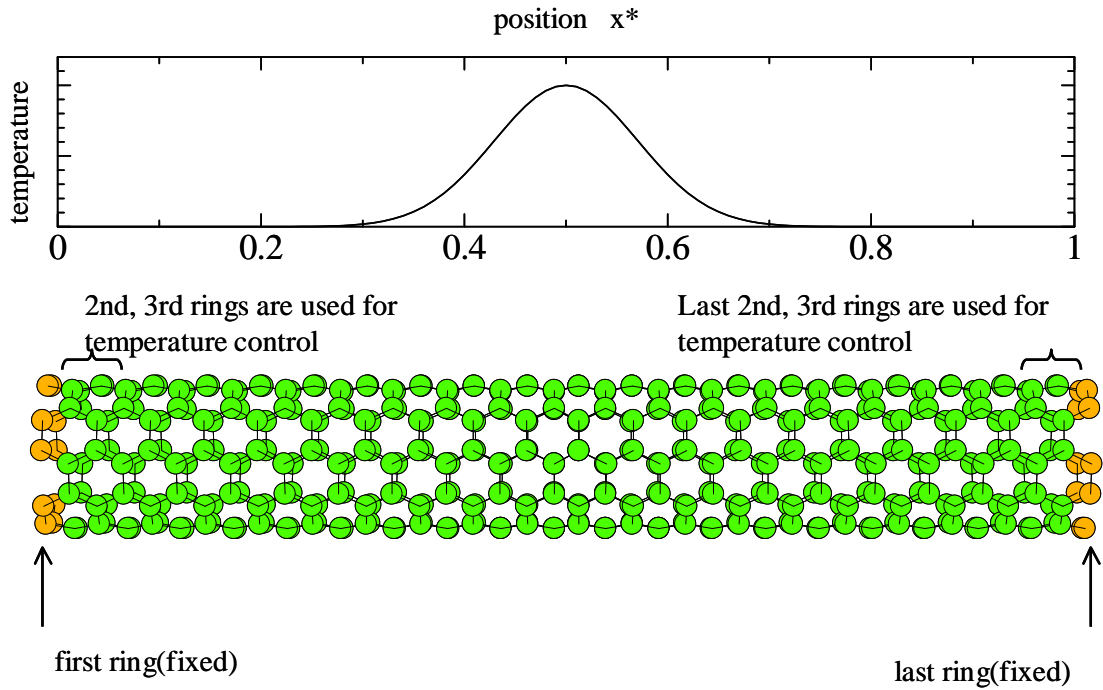


Fig. 3 Schematic of calculation system and temperature profile. Both the ends of the SWCNT are fixed and each of the following two rings is used for temperature control. First, the SWCNT is fully annealed at nearly 0 K using these four rings and then, the temperature profile is given instantly as shown above to express heat propagation.

where  $T_0$  is the maximum temperature at  $t = 0$ ,  $n$  is the ring number,  $n_0$  is the total number of rings, and  $\varepsilon$  is the width of the Gaussian distribution. As shown in Fig. 3, both ends of the SWCNT are fixed in order to attenuate the longitudinal components of heat conduction and clearly express the radial component. During the entire calculation, MD simulations were performed 50 times for different specific initial conditions such as the temperature and length of the SWCNT; in order to reduce the noise and those averages were adopted.

### 3. Results and discussion

Recently, it has become clear that heat conduction in an SWCNT is mainly attributed to phonons, and in particular, to optical phonons. Thus, the behavior of heat propagation indicates non-Fourier heat conduction and thus shows wavy or wavelike thermal responses [26]. Cattaneo [36] and Vernotte [37] subjected SWCNTs to a high-speed process such as ultra short-pulsed laser heating and thus introduced the macroscopic thermal wave model, which is the hyperbolic energy equation, as shown in Eq. (4).

$$\tau \frac{\partial^2 T}{\partial t^2} + \frac{\partial T}{\partial t} = \alpha \nabla^2 T \quad (4)$$

Shiomi and Maruyama [38] elucidated that heat conduction in SWCNTs by

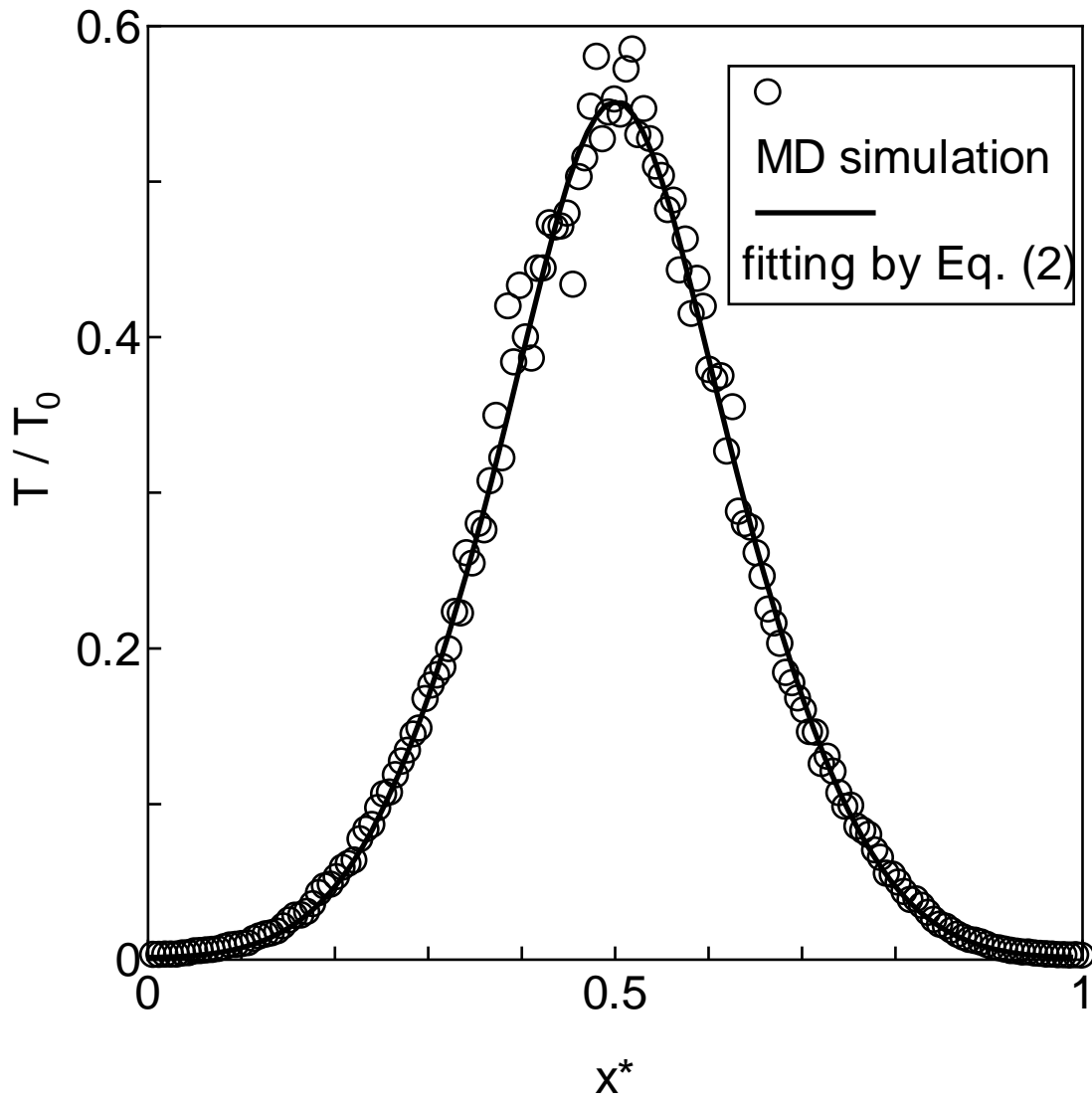


Fig. 4 Temperature profile fitted using Eq. (2). The temperature profile obtained using the MD simulation is fitted using Eq. (2) with two relaxation timescales. The horizontal and vertical axes represent the dimensionless length and dimensionless temperature, respectively.

using the extended macroscopic heat conduction model with two different timescales, which was originally proposed by Tzou [39], as shown in Eq. (2). Figure 4 shows the temperature profile derived using our MD simulation for C1600 SWCNT (200 Å, (5, 5) chirality) at 2.5 K; the thermal diffusivity ( $\alpha$ ) is determined by fitting using Eq. (2). As mentioned above, in this system both the ends are fixed in order to attenuate the longitudinal heat conduction component; thus, the temperature profile must be observed before the heat propagates at the end in order to avoid unpredictable responses. Compared to this good consistency as shown Fig. 4, the temperature profile of the nickel-coated SWCNT cannot be fitted fully by the Eq. (2) as shown in Fig. 5. Figure 5 shows the result for the C1920 SWCNT coated with Ni1076 and it shows two shoulders at  $x^* = 0.15$  and  $0.85$ . This might be attributed to the effect of the other heat flux carried by nickel atoms, which might propagate faster than that of the SWCNT in 240 Å long. As mentioned by Shiomi & Maruyama, the existence of two main heat fluxes result in the failure of fitting using Eq. (2). One of the two reasons why the shoulders are attributed to the effect of nickel atoms is the absence of the shoulder in the longer nickel-coated SWCNT and uncoated SWCNT. The former has higher thermal

diffusivity that leads to concealment of the nickel effect; this is because owing to the thermal interfacial resistance, the contribution of nickel to heat conduction is not very large. The latter does not originally have other heat flux. The other reason is that this shoulder can be fitted by additional thermal diffusivity ( $\alpha$ ) derived using Eq. (4); the fitting line is shown in Fig. 5 (dotted line). This indicates that the total thermal conductivity of the nickel-coated SWCNT should be expressed by the summation of the contributions of SWCNT and nickel, as given below.

$$\begin{aligned}
T &= T_{NT} + \varepsilon \cdot T_m \\
\alpha_m &= \varepsilon \cdot \alpha \\
\lambda &= \lambda_{NT} + \lambda_m = \rho_{NT} C_{v,NT} \alpha_{NT} + \varepsilon \cdot \rho_m C_{v,m} \alpha_m
\end{aligned}
\tag{5}$$

Here,  $\varepsilon$  is the fraction of nickel contribution ( $0 \leq \varepsilon \leq 1$ ), and the temperature

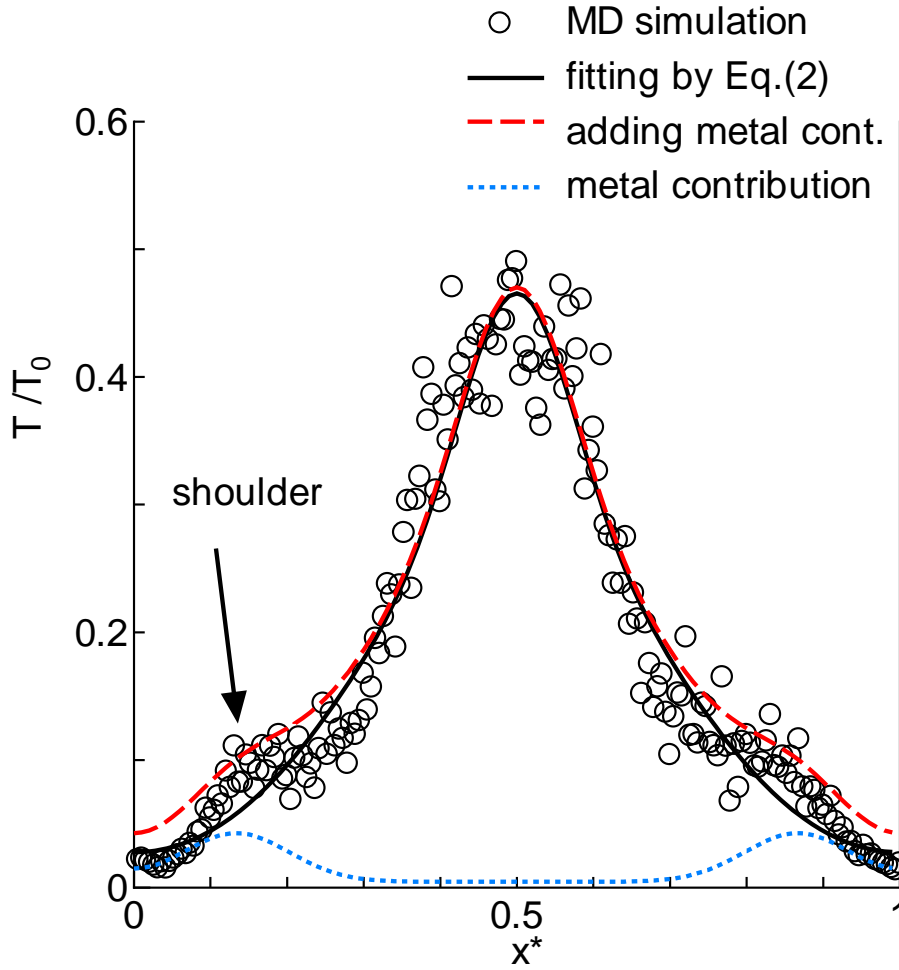


Fig. 5 Temperature profile of nickel-coated SWCNT (C1920 with Ni1076).

The fitting using Eq. (2) results in a failure owing to the shoulders at  $x^* =$

0.15 and 0.85. The shoulders, which might be attributed to the nickel

contribution, which indicate the additional heat flux, obtained using Eq. (4).

profile is expressed by the SWCNT contribution ( $T_{NT}$ ) and the nickel contribution ( $T_m$ ).

In case of Fig. 5,  $\varepsilon$  is approximately 0.1 and the thermal diffusivity ( $\alpha_{Ni}$ ) is  $3.68 \times 10^{-5}$ . Assuming the diameter of the first nickel layer is  $10.5 \text{ \AA}$  and that of SWCNT is  $7 \text{ \AA}$ , the density of nickel is roughly estimated as  $8.5 \times 10^3 \text{ kg/m}^3$  that is slightly smaller than the bulk property ( $8.9 \times 10^3 \text{ kg/m}^3$ ). Finally, the thermal conductivity of nickel layer is expected to be  $25 \text{ W/m}\cdot\text{K}$ .

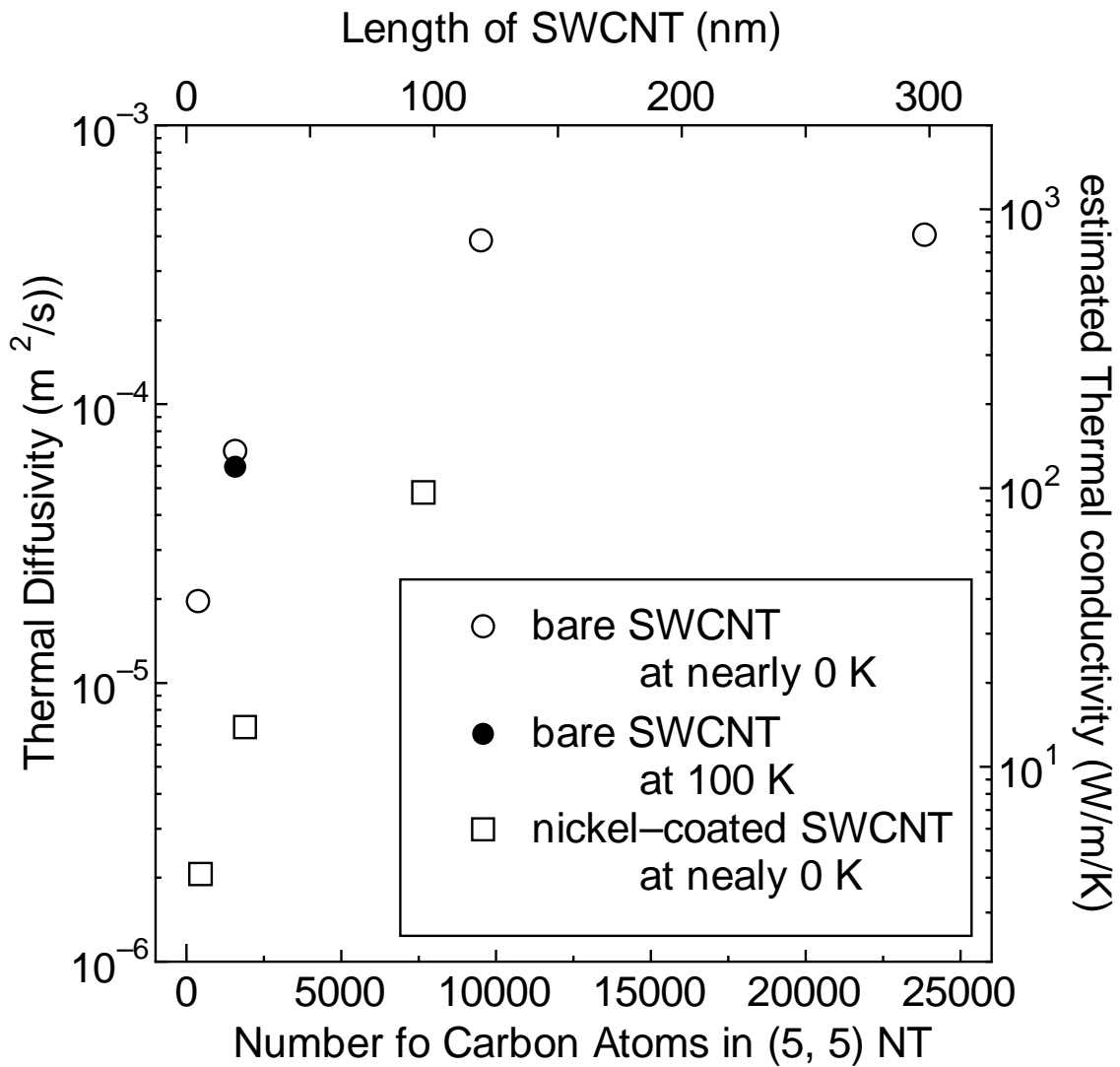


Fig. 6 Thermal diffusivity estimated in this study. The thermal diffusivity of the nickel-coated SWCNT is expressed without nickel layer contribution and decreases by 90%. The estimated thermal conductivity ( $\lambda$ ) is expressed as follows by using thermal diffusivity ( $\alpha$ ):  $\lambda = 1 \times 10^6 \alpha - 3 \times 10^6 \alpha$ . It depends on the definition of the density and specific heat capacity ( $C_v$ ) of the SWCNTs is assumed to be  $3R$ , where  $R$  is a gas constant.

Figure 6 shows the thermal diffusivity of the nickel-coated and uncoated SWCNT at approximately 0 K and 100 K (only for C1600). Consequently, the thermal diffusivity of the nickel-coated SWCNT exhibits approximately 10 times lower than that of an uncoated SWCNT of the same length when it is evaluated without nickel layer contribution. At 100 K, the thermal diffusivity shows consistent decrease, because the thermal vibration disperses the phonon transportation. Most importantly, nickel contributed to heat conduction, as shown by the “shoulder” in Fig. 5 and this value is comparable to that of short length metal-coated SWCNT. Thus, for the short-length SWCNT, the nickel layer is supposed to have comparably large amount of heat conduction together with electron contribution, which is not estimated by MD simulation and that compensates for the decrease in the thermal diffusivity. However, this metal effect might be negligible for longer metal-coated SWCNTs owing to the increase in thermal diffusivity of SWCNT itself. After all, the decrease induced by metal coating does not become a fatal fault in thermal conductivity when it is compared with other conventional devices or materials.

#### 4. Conclusion

The physical properties of nickel-coated SWCNTs were determined using molecular dynamics simulations. The thermal diffusivity of SWCNTs can be determined by applying the hyperbolic equation with two different timescales; the longitudinal mode of the SWCNTs is attenuated by fixing their ends. We found that for the nickel-coated SWCNT, another heat flux is carried by nickel itself. This additional heat flux is not so large owing to the interfacial resistance of carbon-nickel boundary; however, unlike SWCNTs, the heat conduction in the nickel layer does not show length dependence; therefore, when the SWCNT is short, this additional heat flux might compensate for the thermal diffusivity and result in enhancing the total thermal conductivity. In our simulation this nickel contribution is estimated as 25 W/m·K for the short nickel-coated SWCNT (C1920 with Ni1076 SWCNT), and this value is larger than SWCNT itself in this sample.

## References

- [1] S. Iijima, T. Ichihashi, *Nature* 363 (1993) 603.
- [2] K. Hata, D.N. Futaba, K. Mizuno, T. Namai, M. Yumura, S. Iijima, *Science* 306 (2004) 1362.
- [3] R. Krupke, F. Hennrich, von H. Lohneysen, M.M. Kappes, *Science*

301 (2003) 344.

[4] M. Fujii, X. Zhang, H. Xie, H. Ago, K. Takahashi, T. Ikuta, H. Abe, and T. Shimizu, *Phys. Rev. Lett.* 95 (2005) 065502.

[5] R. Zhu, E. Pan and A.K. Roy, *Mater. Sci. Eng. A* 447 (2007) 51.

[6] B. Ashrafi and P. Hubert, *Compos. Sci. Technol.* 66 (2006) 387.

[7] S.K. Pregler, B.W. Jeong and S.B. Sinnott, *Compos. Sci. Technol.* 68 (2008) 2049.

[8] A. H. Barber <sup>1</sup>, S. R. Cohen <sup>2</sup>, A. Eitan <sup>3</sup>, L. S. Schadler <sup>3</sup>, H. D. Wagner., *Adv. Mater.* 18 (2006) 83.

[9] Bing-Xing Yanga, Jia-Hua Shia, K.P. Pramodab and Suat Hong Goha., *Compos. Sci. Technol.* 68 (2008) 2490.

[10] S.P. Xiao and W.Y. Hou, *Phys. Rev. B* 73 (2009) 115406.

[11] H.Y. Song and X.W. Zha, *Physica B* 403 (2008) 559.

[12] C. L. Xu, B. Q. Wei, R. Z. Ma, J. Liang, X. K. Ma and D. H. Wu *Carbon* 37 (1999) 855.

[13] J.Y. Hwanga, A. Neiraa, T.W. Scharfa, J. Tileyb and R. Banerjee, *Scripta Mater.* 59 (2008) 487.

- [14] H.Y. Song and X.W. Zha, *J. Phys. D: Appl. Phys.* 42 (2009) 225402.
- [15] Y.J. Jeong, S.I. Cha, K.T. Kim, K.H. Lee, C.B. Mo, S.H. Hong, *Small* 3 (2007) 840.
- [16] K.T. Kim, S.I. Cha, T. Gemming, J. Eckert, S.H. Hong, *Small* 4 (2008) 1936.
- [17] C.S. Goh, J. Wei, J.C. Leem and M. Gupta, *Nanotechnology* 17 (2006) 7.
- [18] C.S. Goh, J. Wei, J.C. Leem and M. Gupta, *Mater. Sci. Eng. A* 423 (2006) 153.
- [19] E. Carreno-Morelli, J. Yang, E. Couteau, K. Hernadi, J.W. Seo, C. Bonjour, L. Forro, and R. Schaller, *Phys. Status Solidi A* 201 (2004) 53.
- [20] Y. Shimizu, S. Miki, T. Soga, I. Itoh, H. Todoroki, T. Hosono, K. Sakai, T. Hayashi, Y.A. Kim, M. Endo, S. Morimoto, and A. Koide, *Scripta Mater.* 58 (2008) 267.
- [21] Y. Zhang, N.W. Franklin, R.J. Chen, H.J. Dai, *Chem. Phys. Lett.* 331 (2000) 35.
- [22] K. Ishikawa, H.M. Duong, J. Shiomi, S. Maruyama, *Proc. of*

ASME-JSME Thermal Eng. (2007) 32783.

- [23] S. Inoue, Y. Matsumura, Chem. Phys. Lett. 469 (2009) 125.
- [24] S. Nuno, Int. J. Solid and Structures 45 (2008) 4902.
- [25] Z. Xu and M.J. Buehler, ACS Nano 3 (2009) 2767.
- [26] D.W. Tang, N. Araki, Int. J. Heat Mass Trans. 42 (1999) 855.
- [27] S. Inoue, Y. Matsumura, Chem. Phys. Lett. 464 (2008) 160.
- [28] P.M. Morse, Phys. Rev. 34 (1929) 57.
- [29] M.W. Finnis, J.E. Sinclair, Philos. Mag. A 50 (1984) 45.
- [30] M.S. Daw, M.I. Baskes, Phys. Rev. B 42 (1984) 6443.
- [31] K.D. Nielson, A.C.T. van Duin, J. Oxgaard, W.-Q. Deng, and W.A. Goddard III, J. Phys. Chem. A 109 (2005) 493.
- [32] D.W. Brenner, Phys. Rev. B 42 (1990) 9458.
- [33] Y. Yamaguchi, S. Maruyama, Chem. Phys. Lett. 286 (1998) 336.
- [34] Y. Shibuta, S. Maruyama, Comput. Mat. Sci. 39 (2007) 842.
- [35] S. Inoue, Y. Matsumura, Carbon 46 (2008) 2046.
- [36] C. Cattaneo, Comptes 247 (1958) 431.
- [37] P. Vernotte, Comptes 246 (1958) 3154.
- [38] J. Shiomi, S. Maruyama, Phys. Rev. B 73 (2006) 205420.

- [39] D.Y. Tzou, *J. Heat Transf. ASME* 117 (1995) 8.

## Figure Captions

Fig. 1 Example of calculated object (C480 with Ni269). The SWCNT is completely covered with nickel atoms (blue).

Fig. 2 Schematic of the position of nickel deposition onto SWCNT sidewall (expressed using unfolded graphite sheet). The distance of nickel (2.494 Å) is quite comparable to the equilibrium bond length for Ni-Ni.

Fig. 3 Schematic of calculation system and temperature profile. Both the ends of the SWCNT are fixed and each of the following two rings is used for temperature control. First, the SWCNT is fully annealed at nearly 0 K using these four rings and then, the temperature profile is given instantly as shown above to express heat propagation.

Fig. 4 Temperature profile fitted using Eq. (2). The temperature profile obtained using the MD simulation is fitted using Eq. (2) with two relaxation timescales. The horizontal and vertical axes represent the dimensionless length and dimensionless temperature, respectively.

Fig. 5 Temperature profile of nickel-coated SWCNT (C1920 with Ni1076). The fitting using Eq. (2) results in a failure owing to the shoulders at

$x^* = 0.15$  and  $0.85$ . The shoulders, which might be attributed to the nickel contribution, which indicate the additional heat flux, obtained using Eq. (4).

Fig. 6 Thermal diffusivity estimated in this study. The thermal diffusivity of the nickel-coated SWCNT is expressed without nickel layer contribution and decreases by 90%. The estimated thermal conductivity ( $\lambda$ ) is expressed as follows by using thermal diffusivity ( $\alpha$ ):  $\lambda = 1 \times 10^6 \alpha - 3 \times 10^6 \alpha$ . It depends on the definition of the density and specific heat capacity ( $C_p$ ) of the SWCNTs is assumed to be  $3R$ , where  $R$  is a gas constant.